Local determination of weak anisotropy parameters from a walkaway VSP data [1]

Xuyao Zheng[*)], **Ivan Pšenčík**[*)], **Steve Horne**[**)] and **Scott Leaney**[**)]

[*)] *Geophysical Institute, Acad.Sci.of Czech Republic, Boční II, Praha 4, Czech Republic, e-mail: zheng@ig.cas.cz, ip@ig.cas.cz*
[**)] *Schlumberger, Buckingham Gate, Gatwick, RH6 0NZ, UK, e-mail: shorne@slb.com, leaney@slb.com*

ABSTRACT

We apply the inversion scheme of Zheng and Pšenčík (2001) to the walkaway VSP data. The most important difference from the application in Zheng and Pšenčík (2001) is that the data are collected along a single profile so that we are able to describe anisotropy only in the vertical plane containing the profile. Another important aspect is that we know only vertical components of polarization vectors and we have to assume that the vectors are confined to the vertical plane containing the profile. We test first the inversion scheme on synthetic data. We consider two models of transversely isotropic (TI) medium with axis of symmetry deviating from vertical. The qP-wave anisotropy of the models is 8% and 16%. We show that the vertical sections of qP-wave phase velocity can be recovered very reliably for both anisotropies even if 10% noise is added to data. Then we apply the inversion scheme to the walkaway VSP data of Horne and Leaney (2000) collected in the Java Sea region. The data are inverted first without making any assumption about the medium, then assuming that the medium is transversely isotropic with vertical axis of symmetry (VTI), i.e., with the assumption also made by Horne and Leaney (2000) in their inversion. In both cases anisotropy of slightly lower strength is obtained than by Horne and Leaney (2000). In the first case, the recovered medium is close to TI but its axis is tilted.

INTRODUCTION

We apply the inversion scheme of Zheng and Pšenčík (2001) to the walkaway VSP data. For the determination of WA parameters (for the definition of WA parameters see Appendix A, Eqs.(A3)) we use Eq.(22) of Zheng and Pšenčík (2001):

$$(\alpha^2-\beta^2)^{-1}(B_{13}X^{(2)}-B_{23}X^{(1)})-\frac{1}{2}\alpha^{-2}B_{33}\eta=$$

[1]Seismic Waves in Complex 3-D Structures, Report 11 (Department of Geophysics, Charles University, Prague 2001), pp.43-68

$$(X^{(2)}e_i^{(1)} - X^{(1)}e_i^{(2)})g_i + \alpha\Delta\eta(X^{(1)}e_3^{(2)} - X^{(2)}e_3^{(1)} + \alpha\eta^2). \tag{1}$$

The symbols α and β denote the P and S wave velocities of the isotropic reference medium. The symbols B_{mn} denote elements of the *weak anisotropy* matrix,

$$B_{mn} = a_{ijkl}e_i^{(m)}e_j^{(3)}e_l^{(3)}e_k^{(n)} - c_0^2\delta_{mn}, \tag{2}$$

in which c_0 stands for α $(m = n = 3)$ or β $(m = n = 1, 2)$. The symbol $X^{(K)}$, $(K = 1, 2)$ is defined as

$$X^{(K)} = \xi e_2^{(K)} - \zeta e_1^{(K)}. \tag{3}$$

The symbols ξ and ζ denote sizes of radial and transverse projections of the slowness vector p_i^0 in the reference medium. The vectors $e_i^{(1)}$, $e_i^{(2)}$ and $e_i^{(3)}$ are three mutually perpendicular unit vectors, the vector $e_i^{(3)}$ being parallel to the polarization vector and phase normal of the P wave in the reference isotropic medium. Thus, $p_i^0 = \alpha^{-1}e_i^{(3)}$. The WA parameters appear in Eq.(1) through the elements of the weak anisotropy matrix B_{mn}, see Appendix A. The free surface effects are neglected throughout the study.

We test first the inversion scheme on synthetic data. We consider two models of laterally inhomogeneous, transversely isotropic (TI) media with axis of symmetry deviating at the top of the model by 20^o from vertical and vertical axis of symmetry at the bottom of the model. The qP-wave anisotropy of the first model is 8%, of the other 16%. Anisotropy is defined as a difference of the maximum and minimum qP-wave phase velocities divided by their average. The situation resembles the experiment with real data shown in the second part of this paper. We use vertical components of observed slowness and polarization vectors to determine weak anisotropy (WA) parameters by solving system of equations (1). Because we have available data from a single profile only, we can recover only 5 qP-wave WA parameters from 15, describing a general weakly anisotropic medium (Pšenčík and Gajewski, 1998). These five parameters are ϵ_x, ϵ_z, δ_x, ϵ_{15} and ϵ_{35}. From these parameters, vertical sections of qP-wave phase velocity can be constructed. We invert noise-free synthetics and synthetics with 10% Gaussian noise.

In the second part, we apply the inversion scheme to the walkaway VSP data of Horne and Leaney (2000) collected in the Java region. The data contain information on downgoing and upgoing (reflected) qP and qS waves. In this study, we concentrate on the information related to the qP waves only. The data are inverted first without making any assumption about the medium, then assuming that the medium is transversely isotropic with vertical axis of symmetry (VTI), i.e., with the assumption made by Horne and Leaney (2000) in their inversion.

The P-wave velocity α of the reference isotropic medium is determined from the data for downgoing qP wave from the interval of polar angles (0^0, 75^0) using the formula

$$\alpha = \frac{1}{N}\sum_{i=1}^{N}\frac{g_{z(i)}}{p_{z(i)}}. \tag{4}$$

In (4), p_z and g_z are the vertical components of the slowness and polarization vectors, N is the number of data used.

The SVD algorithm is used to solve the system of equations resulting from Eq.(1), both for synthetic and real data.

SYNTHETIC TESTS

For the following tests we use the VSP configuration similar to that used by Zheng and Pšenčík (2001) in their multiazimuthal study. The whole model is confined in a model box whose horizontal dimensions are 10 × 10 km. The borehole is situated in the center of the model. A single surface profile is considered. The top surface of the model box is horizontal and situated at the depth of $z = 0$km. The bottom surface is an inclined plane intersecting the vertical border of the model $x = -5$km at the depth of 9km and the border $x = 5$km at the depth of 1km. Two models of laterally inhomogeneous TI media with inclined axes of symmetry whose inclination varies are considered. The axes of symmetry at the top surface are rotated in the (x, z)-plane by 20^o from the z-axis, and then by 25^o around the z-axis. The axes of symmetry at the bottom surface are vertical. Between the top and the bottom surfaces the elastic parameters are determined by linear interpolation. The inclined bottom surface introduces lateral inhomogeneity and variation of anisotropy into the models.

Anisotropy of the first model is 8%. We call this model TI-08. At the top of the model, the density-normalized elastic parameters A_{ij}, in $(\mathrm{km/s})^2$ in the unrotated crystal coordinate system are: $A_{11} = A_{22} = 15.71$, $A_{33} = 13.39$, $A_{12} = 5.05$, $A_{13} = A_{23} = 4.46$, $A_{44} = A_{55} = 4.98$. At the bottom of the model: $A_{11} = 35.35$, $A_{33} = 30.13$, $A_{12} = 11.36$, $A_{13} = 10.04$, $A_{44} = 11.21$.

Anisotropy of the second model is 16%. We call this model TI-16. At the top of the model, the density-normalized elastic parameters A_{ij}, in $(\mathrm{km/s})^2$ in the unrotated crystal coordinate system are: $A_{11} = A_{22} = 18.02$, $A_{33} = 13.39$, $A_{12} = 6.00$, $A_{13} = A_{23} = 5.30$, $A_{44} = A_{55} = 4.46$. At the bottom of the model: $A_{11} = 40.55$, $A_{33} = 30.13$, $A_{12} = 13.54$, $A_{13} = 11.96$, $A_{44} = 10.06$.

The walkaway VSP profile contains 16 sources at each side of the borehole, starting at 0.1 km from the mouth of the borehole. The sources are separated by 0.1 km. The vertical borehole contains 13 three-component receivers starting at a depth of 0.1 km and separated by 0.05 km. In the following, we concentrate on results at three selected receivers, 4, 7 and 10 situated at depths z=0.25, 0.4 and 0.55 km, respectively. The values of the exact WA parameters at these receivers are given in Table 1.

We use the program package ANRAY (Gajewski and Pšenčík, 1990) to generate "observed" synthetic seismograms. The vertical components of slowness and polarization vectors of a downgoing qP wave are determined in the way described by Zheng and Pšenčík (2001). This configuration yields 32 independent equations for 5 WA parameters specifying anisotropy in the vertical plane containing the VSP profile.

Figure 1 shows comparison of results of inversion with observed data for the three selected receivers, 4 (top), 7 (middle) and 10 (bottom) in the model TI-08. The horizontal axes are specified by the polarization angle. The vertical axes show the ratio of $\alpha p_z/g_z$, where p_z

denotes the vertical component of the slowness vector and g_z the vertical component of the polarization vector. The quantity $\alpha p_z/g_z$ represents, approximately, ratio of the vertical components of the phase normal and of the polarization vector. The crosses denote the observed data. The solid curves correspond to the true model and the dotted horizontal lines to the reference isotropic medium, in which the phase normal and polarization vector are always equal. The dashed curves represent results of the inversion. We can see perfect coincidence of true, observed and inverted results.

Figure 2 shows the same but for stronger anisotropy, for the model TI-16. We can observe slight deviations of the observed data from the true data for larger angles of incidence (in such a case αp_z and g_z become small). Results of inversion, however, practically coincide with the true model data.

Figure 3 shows the same as Figure 1, but now for seismograms with 10% noise. The deviations of observed data from the true data for larger angles of incidence are more pronounced now and cause slight differences of inverted results from the true ones. This can be seen especially at the middle receiver for larger angles of incidence. This effect is even more pronounced in Figure 4 showing results for the noisy data for the model TI-16.

Figure 5 shows comparison of the true and inverted sections of the phase velocity surfaces by the vertical plane containing the VSP profile for the model TI-08. The left column shows results of inversion of the noise-free synthetics, the right column shows results of inversion of synthetics with 10% noise. As before, results for three selected receivers, 4 (top), 7 (middle) and 10 (bottom) are shown. The solid curves show the true sections, the dashed curves the inverted sections. Empty circles and the symbols $\times$ indicate positions of the true and inverted minimum phase velocity, respectively. Except the shallowest receiver 4 (insufficient illumination), the results confirm what we could see in Figure 1: perfect fit of the true and inverted sections as well as positions of minimum velocities.

Figure 6 shows the same as Figure 5 but for the model TI-16 with stronger anisotropy. We can again see, now slightly stronger, discrepancies between true and inverted sections at the shallowest receiver but reasonably good fit for deeper (especially for the deepest and best illuminated) receivers no matter if noise-free or noisy synthetics are used.

Figure 7 shows the relative errors of the inverted parameters for the noise-free data obtained for the model TI-08. Each figure shows 3 bar charts corresponding to the receiver 4 (top), 7 (middle) and 10 (bottom). The values of the exact WA parameters for these receivers are given in Table 1. Comparison of errors for individual receivers confirms what we observed in previous figures. Accuracy is, generally increasing with depth. This can be especially clearly seen on the WA parameter ϵ_x. Large relative errors of the parameter δ_x are caused by its negligible size, see Table 1. If, instead of the errors of WA parameters, relative errors of the corresponding elastic parameters or their combinations are shown, the relative errors considerably reduce, see Figure 8. The relative errors of the elastic parameters, except the parameter A_{35}, are less than 5%.

Figure 9 shows the same as Figure 7 but for noisy data. We can see that the noise affected accuracy of determination of WA parameters at the receivers 4 and 7. At the receiver 10, we can, however, observe only negligible effects. This is a consequence of better illumination of the receiver 10 than of the two shallower receivers.

Figure 10 shows the same as Figure 7 but for the TI-16 model. We can see that the relative errors of inversion for stronger anisotropy are comparable with relative errors of inversion for the model TI-08, for the deepest receiver even higher.

Figure 11 shows the same as Figure 10 but for noisy data. As in the case of the model TI-08, we can see that added noise does not affect much the accuracy of the inversion. On the contrary, some parameters are even determined with higher accuracy.

The above synthetic tests including even noisy data indicate that the proposed inversion procedure of a walkaway data yields reasonably accurate results although data of only downgoing qP waves were used. Although some of the WA parameters are determined with lower precision, the form of the section of the phase velocity surface by the vertical plane containing the profile is recovered correctly including positions of minimum velocities.

INVERSION OF REAL DATA

Let us now apply the above inversion scheme to the walkaway VSP data of Horne and Leaney (2000) collected in the Java Sea region. Vertical components of slowness and polarization vectors of downgoing and upgoing (reflected) qP and qS waves were determined using the parametric inversion approach of Esmersoy (1990) and Leaney (1990). In this study, we concentrate on the information related to the qP waves only. No assumptions are made about the horizontal components of the slowness vector. The polarization vector is assumed to be confined to the vertical plane containing the profile and the borehole. The waves are generated by 228 sources distributed along a single profile on the Earth's surface. If we identify the profile with the x-axis of a right-handed Cartesian coordinate system, whose z-axis coincides with the borehole and is positive downwards, the sources extend from -2.5 to 2.5km with approximately 25m spacing.

We make two experiments. In the first, denoted by A, we make no assumptions about the anisotropy of the medium. Because we have available data from a single profile only, we can again recover only 5 WA parameters ϵ_x, ϵ_z, δ_x, ϵ_{15} and ϵ_{35}. In the second experiment, denoted by B, we assume that the studied medium is VTI and is thus specified by only 3 WA parameters ϵ_x, ϵ_z and δ_x.

We have data for 228 downgoing and upgoing qP waves available. For the inversion, we select data for 133 downgoing and 170 upgoing waves with polarization angles within the interval $(0^o, 75^o)$. The data from outside the interval are less reliable because the vertical components of the slowness and polarization vectors for these angles are small. We have thus a system of 133 equations if only downgoing qP wave is considered and 303 equations if both downgoing and upgoing waves are considered. We solve these equations for the above 5 or 3 WA parameters.

Using Eq.(4), the reference velocity for the experiment A is found to be α=2.75 km/s. Around this value we take an interval of reference velocities from 2.3 to 3.3 km/s, with the step of 0.05 km/s. For these velocities, we calculate quadratic errors of vertical components of the slowness vectors from the difference of observed (obs) and calculated (cal) quantities

$$\sigma^2 = \sum_{i=1}^{N} (p_{z(i)}^{obs} - p_{z(i)}^{cal})^2 \tag{5}$$

Results are shown by crosses in Fig.12 (calculation of each point in Fig.12 requires only several seconds of CPU time). The square (at the upper margin of the plot) and triangle are errors corresponding to two models: (a) c_{11}=11.19, c_{33}=7.62, c_{55}=1.81, c_{13}=4.05 and (b) c_{11}=11.35, c_{33}=8.56, c_{55}=1.81, c_{13}=4.40. Both models are deduced from the data in Tab.2 of Horne and Leaney (2000). (Note the high V_P/V_S ratio.) The model (a) corresponds to the slowness inversion, the model (b) to the combined slowness and polarization inversion. The $\times$ symbol corresponds to the VTI model considered in the experiment B. The circled cross corresponds to the optimum reference model considered in the experiment A.

Experiment A

Fig.13 shows a plot of vertical components of the slowness vector versus polarization angle in the way used by Horne and Leaney (2000). In the upper frame observed data ($\times$) are compared with the curve corresponding to the inversion of all qP waves (up- and downgoing) in the experiment A. The crosses indicate a complete set of observed data. The crosses with positive values of the vertical component of the slowness vector correspond to the downgoing qP wave, the crosses with negative values correspond to upgoing qP wave. In the lower frame, curves corresponding to various inversions are shown. The thin and thick solid curves correspond to the results of the experiment A. The thin curve is obtained from downgoing qP waves only, the thick curve from both downgoing and upgoing qP waves. The two dashed curves correspond to slowness (19) and polarization (14) inversion of Horne and Leaney (2000) who assumed the medium to be VTI. We can see that all four curves are nearly identical, no matter how general is the model.

In order to differentiate more individual solutions shown in Fig.13, we display the data in a different way in Figure 14. Horizontal axes are specified again by the polarization angle. The vertical axis shows the ratio of $\alpha p_z/g_z$. The crosses denote again the real data, in the upper plot for the downgoing wave, in the lower plot for upgoing wave. We can see that the data are now more dispersed than in Figure 13. If we compare upper and lower plots, we can see greater dispersion in the lower plot indicating that the picking error of data related to upgoing waves is higher, see Horne and Leaney (2000). The thick curves in Figure 14 have the same meaning as in Figure 13. The thin line in the upper plot is obtained from downgoing qP wave only, the thin line in the lower plot from upgoing qP wave only. The horizontal dotted line corresponds to the isotropic reference model, in which the phase normal and polarization vector are always equal. From comparison of the presented curves, it is evident that the solid lines are non-symmetric in contrast to dashed curves which are symmetric. This indicates that the longitudinal axis of the medium described by solid curves is not vertical as in the case of the VTI medium of Horne and Leaney (2000). This can be clearly seen in Figure 15.

Figure 15 shows the sections of several phase velocity surfaces by the vertical plane (x, z). Dashed lines show two elliptical sections corresponding to VTI models of Horne and Leaney (2000). The two models differ by vertical velocity. The horizontal velocity, which is larger is the same for both models. The thin and thick solid curves show results obtained by solving Eq.(1) for only downgoing waves and for both downgoing and upgoing waves, respectively. The two solid curves seem to indicate weaker anisotropy (at least in the shown section) than the curves of Horne and Leaney (2000). In contrast to Horne and Leaney's anisotropy of approximately 14% and 19%, use of the formula (1) yields anisotropy of about 8%. The open circles indicate minima of velocity on solid curves. They represent, very probably, projections of longitudinal axes into the plane (x, z). We can see that the minimum velocity does not correspond to vertical direction as in the case of the Horne and Leany (2000) inversion and, moreover, it seems that the longitudinal axis deviates from the plane of Figure 15. For its specification, data from, at least, another profile would be necessary.

In order to explain the observed differences between results of Horne and Leaney (2000) and results of this study (strength of anisotropy, orientation of the axis of symmetry) we plan to evaluate errors of the inverted parameters. We also intend to use the available qS-wave data.

Experiment B

Figure 16 shows, in the same display as Figure 14, the results of inversion made under assumption that the studied medium has VTI symmetry, i.e., under the assumption used also by Horne and Leaney (2000). This fact is reflected in the symmetry of the plot.

Figure 17 shows the sections of the phase velocity surfaces by the vertical plane (x, z). The notation is the same as in Figure 15. The anisotropy found by inverting Eq.(1) is now about 6%, it is again considerably smaller than the anisotropy found by Horne and Leaney (2000).

REFERENCES

Esmersoy,C. (1990), *Inversion of P and SV waves from multicomponent offset vertical seismic profiles*, Geophysics, *55*, 39-50.

Gajewski,D. and Pšenčík,I. (1990), *Vertical seismic profile synthetics by dynamic ray tracing in laterally varying layered anisotropic structures*, J.Geophys.Res., *95*, 11301-11315.

Horne,S.A. and Leaney,S. (2000), *Polarization and slowness component inversion for TI anisotropy*, Geophysical Prospecting, *48*, 779-788.

Leaney,W.S., *Parametric wavefield decomposition and applications*, In *Expanded Abstracts, 60th Ann. Internat. Mtg.*, (Soc.Expl.Geophys., Tulsa 1990) pp. 1097-1100.

Pšenčík,I. and Gajewski,D. (1998), *Polarization, phase velocity and NMO velocity of qP waves in arbitrary weakly anisotropic media*, Geophysics, *63*, 1754-1766.

Zheng,X. and Pšenčík,I.. (2001), *Local determination of weak anisotropy parameters from qP-wave slowness and particle motion measurements.* In: Seismic Waves in Complex 3-D Structures, Report 11, pp.15-42, Dept.of Geophysics, Charles University Prague.

APPENDIX A

The elements B_{33}, B_{13} and B_{23} of the weak anisotropy matrix for an anisotropic medium of arbitrary symmetry read, see Pšenčík and Gajewski (1998):

$$
\begin{aligned}
B_{33} = 2\alpha^2[\epsilon_z n_3^4 &+ 2n_3^3(\epsilon_{34}n_2 + \epsilon_{35}n_1) + n_3^2(\delta_x n_1^2 + \delta_y n_2^2 + 2\chi_z n_1 n_2) \\
&+2n_3(\chi_x n_1^2 n_2 + \chi_y n_1 n_2^2 + \epsilon_{15}n_1^3 + \epsilon_{24}n_2^3) + \epsilon_x n_1^4 + \delta_z n_1^2 n_2^2 \\
&+\epsilon_y n_2^4 + 2\epsilon_{16}n_1^3 n_2 + 2\epsilon_{26}n_1 n_2^3],
\end{aligned} \tag{A1a}
$$

$$
\begin{aligned}
B_{13} = \alpha^2 D^{-1}\Big[&2\epsilon_z n_3^5 + n_3^4(\epsilon_{34}n_2 + \epsilon_{35}n_1) + n_3^3(\delta_x n_1^2 + \delta_y n_2^2 + 2\chi_z n_1 n_2 - 2\epsilon_z) \\
&+n_3^2[(4\chi_x - 3\epsilon_{34})n_1^2 n_2 + (4\chi_y - 3\epsilon_{35})n_1 n_2^2 + (4\epsilon_{15} - 3\epsilon_{35})n_1^3 + (4\epsilon_{24} - 3\epsilon_{34})n_2^3] \\
&+n_3[(2\delta_z - \delta_x - \delta_y)n_1^2 n_2^2 + 2(2\epsilon_{16} - \chi_z)n_1^3 n_2 + 2(2\epsilon_{26} - \chi_z)n_1 n_2^3 + (2\epsilon_x - \delta_x)n_1^4 + (2\epsilon_y - \delta_y)n_2^4] \\
&-\chi_x n_1^2 n_2 - \chi_y n_1 n_2^2 - \epsilon_{15}n_1^3 - \epsilon_{24}n_2^3\Big]
\end{aligned} \tag{A1b}
$$

and

$$
\begin{aligned}
B_{23} = \alpha^2 D^{-1}\Big[&n_3^3(\epsilon_{34}n_1 - \epsilon_{35}n_2) + n_3^2[(\delta_y - \delta_x)n_1 n_2 + \chi_z n_1^2 - \chi_z n_2^2] \\
&+n_3[(2\chi_y - 3\epsilon_{15})n_1^2 n_2 - (2\chi_x - 3\epsilon_{24})n_1 n_2^2 + \chi_x n_1^3 - \chi_y n_2^3] \\
&+(\delta_z - 2\epsilon_x)n_1^3 n_2 + (2\epsilon_y - \delta_z)n_1 n_2^3 + 3(\epsilon_{26} - \epsilon_{16})n_1^2 n_2^2 + \epsilon_{16}n_1^4 - \epsilon_{26}n_2^4\Big].
\end{aligned} \tag{A1c}
$$

The quantity D is defined as

$$D = (n_1^2 + n_2^2)^{1/2}. \tag{A2}$$

The WA parameters appearing in (A1) are defined as follows

$$
\begin{gathered}
\epsilon_x = \frac{A_{11} - \alpha^2}{2\alpha^2}, \quad \epsilon_y = \frac{A_{22} - \alpha^2}{2\alpha^2}, \quad \epsilon_z = \frac{A_{33} - \alpha^2}{2\alpha^2}, \\
\delta_x = \frac{A_{13} + 2A_{55} - \alpha^2}{\alpha^2}, \quad \delta_y = \frac{A_{23} + 2A_{44} - \alpha^2}{\alpha^2}, \quad \delta_z = \frac{A_{12} + 2A_{66} - \alpha^2}{\alpha^2}, \\
\chi_x = \frac{A_{14} + 2A_{56}}{\alpha^2}, \quad \chi_y = \frac{A_{25} + 2A_{46}}{\alpha^2}, \quad \chi_z = \frac{A_{36} + 2A_{45}}{\alpha^2}, \\
\epsilon_{15} = \frac{A_{15}}{\alpha^2}, \quad \epsilon_{16} = \frac{A_{16}}{\alpha^2}, \quad \epsilon_{24} = \frac{A_{24}}{\alpha^2}, \quad \epsilon_{26} = \frac{A_{26}}{\alpha^2}, \quad \epsilon_{34} = \frac{A_{34}}{\alpha^2}, \quad \epsilon_{35} = \frac{A_{35}}{\alpha^2}.
\end{gathered} \tag{A3}
$$

WA		TI-08			TI-16	
	rec. 4	rec. 7	rec. 10	rec. 4	rec. 7	rec. 10
ϵ_x	.0282	.0290	.0298	.0577	.0596	.0614
ϵ_y	.0218	.0231	.0242	.0416	.0446	.0473
ϵ_z	-.0256	-.0265	-.0273	-.0511	-.0519	-.0527
δ_x	.0007	.0002	-.0002	-.0133	-.0169	-.0204
δ_y	-.0030	-.0032	-.0034	-.0007	-.0051	-.0093
δ_z	.0505	.0525	.0544	.1046	.1091	.1133
χ_x	-.0267	-.0250	-.0234	-.0608	-.0569	-.0533
χ_y	-.0185	-.0173	-.0162	-.0334	-.0313	-.0293
χ_z	-.0058	-.0054	-.0051	.0200	.0187	.0175
ϵ_{15}	-.0204	-.0191	-.0178	-.0532	-.0498	-.0467
ϵ_{16}	-.0101	-.0095	-.0089	-.0264	-.0247	-.0232
ϵ_{24}	-.0273	-.0255	-.0239	-.0675	-.0632	-.0592
ϵ_{26}	-.0099	-.0093	-.0087	-.0246	-.0230	-.0215
ϵ_{34}	-.0242	-.0226	-.0212	-.0340	-.0318	-.0298
ϵ_{35}	-.0177	-.0166	-.0155	-.0249	-.0233	-.0219

Table 1

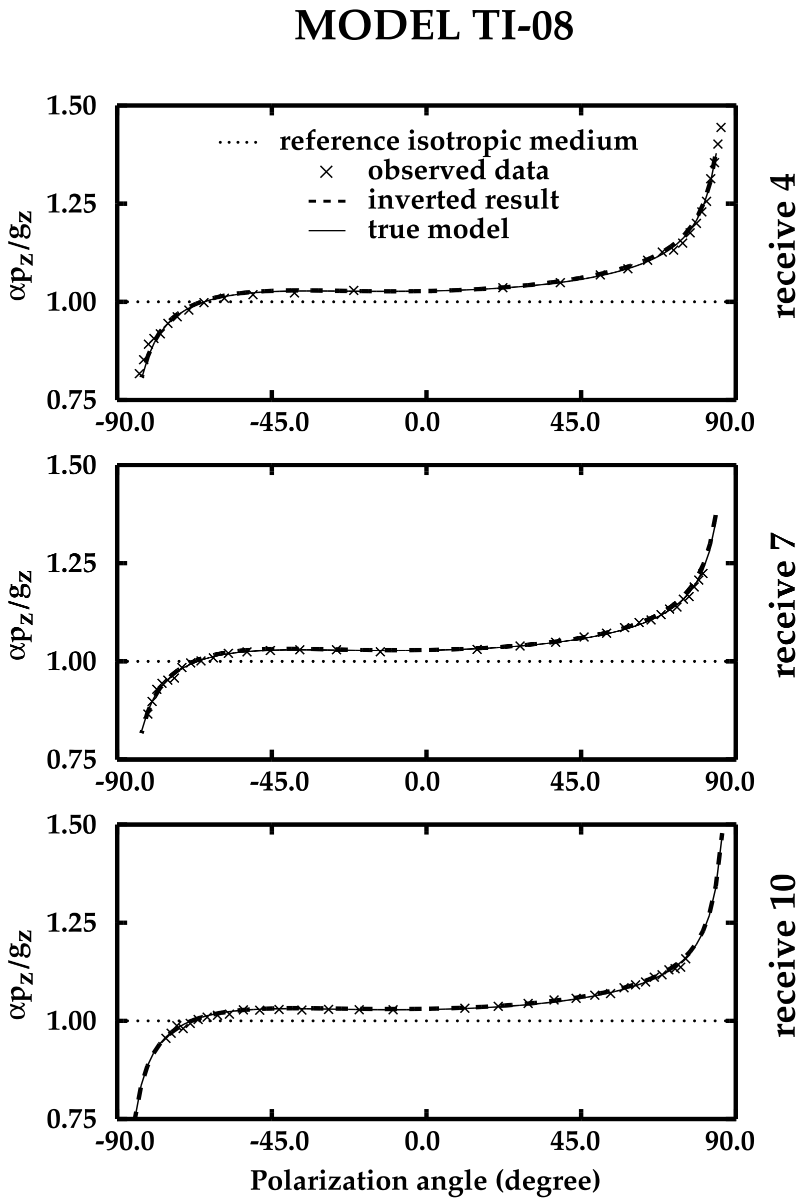

MODEL TI-08
reference isotropic medium
observed data
inverted result
true model
$\alpha p_z/g_z$
1.50
1.25
1.00
0.75
-90.0
-45.0
0.0
45.0
90.0
receive 4
receive 7
receive 10
Polarization angle (degree)

Figure 1

MODEL TI-16

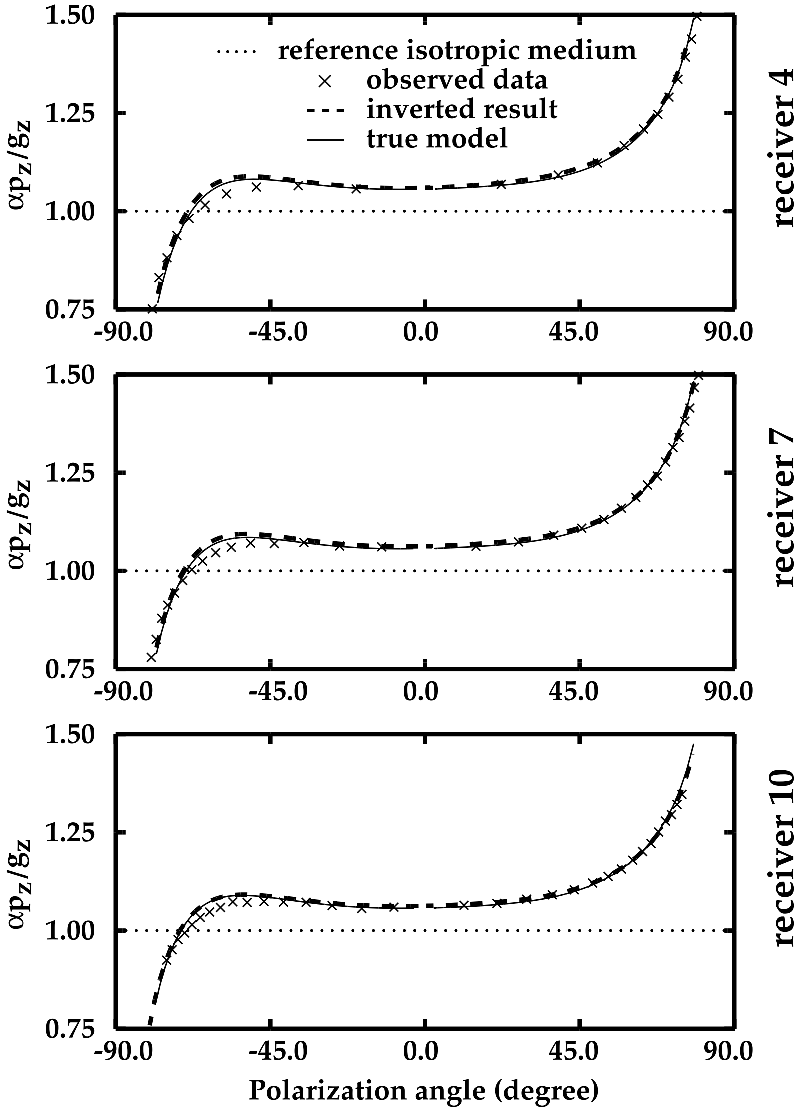

Figure 2

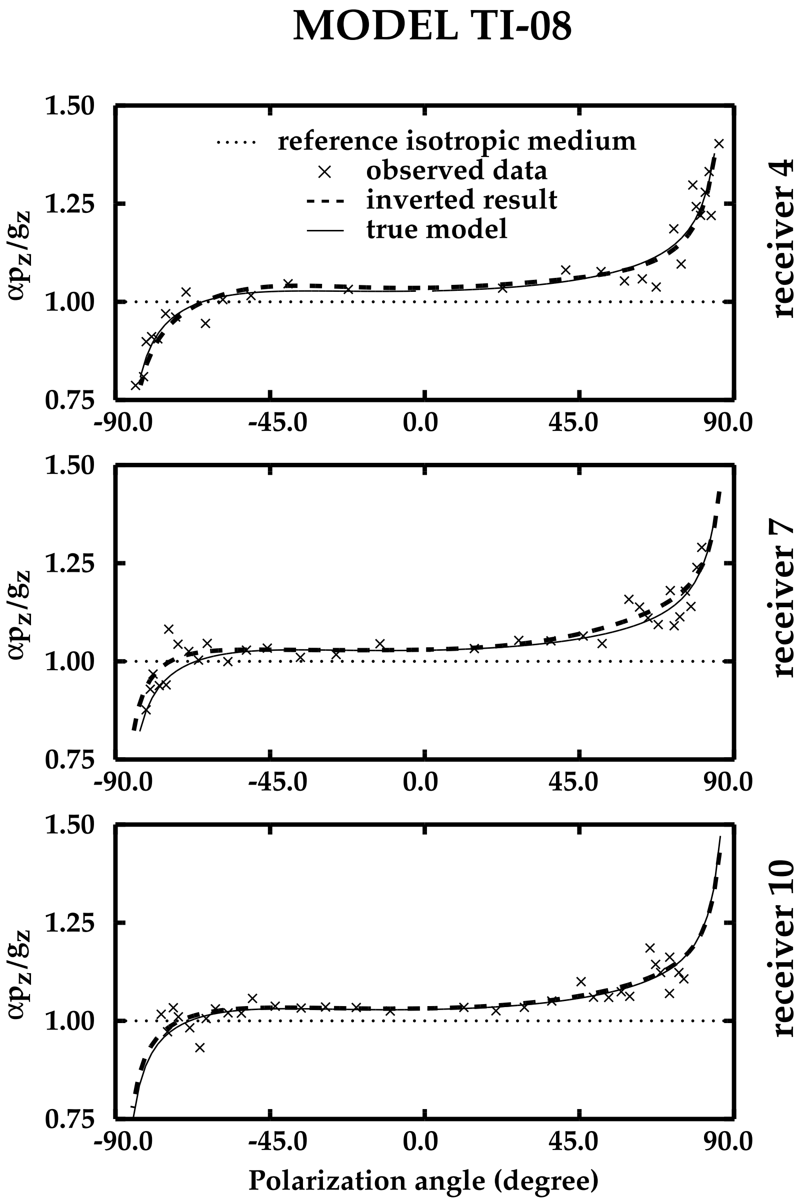
MODEL TI-08
reference isotropic medium
observed data
inverted result
true model
receiver 4
receiver 7
receiver 10
αpz/gz
1.50
1.25
1.00
0.75
-90.0
-45.0
0.0
45.0
90.0
Polarization angle (degree)

Figure 3

MODEL TI-16

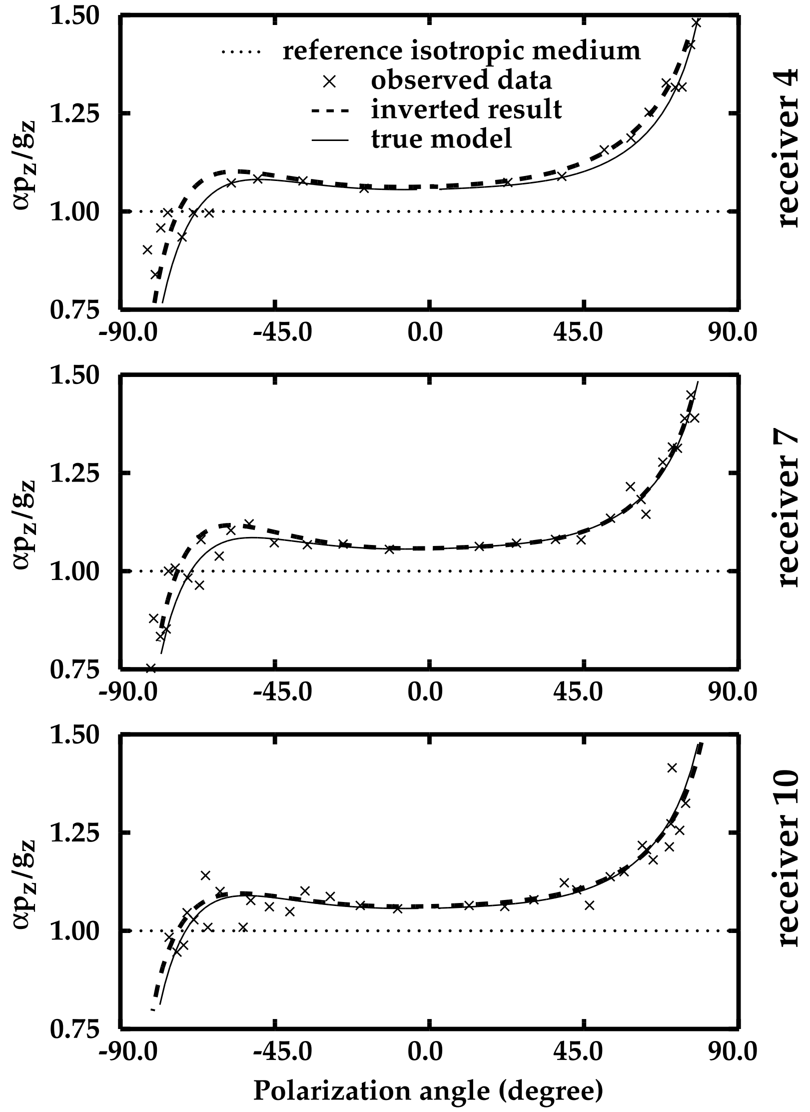

Figure 4

MODEL TI-08

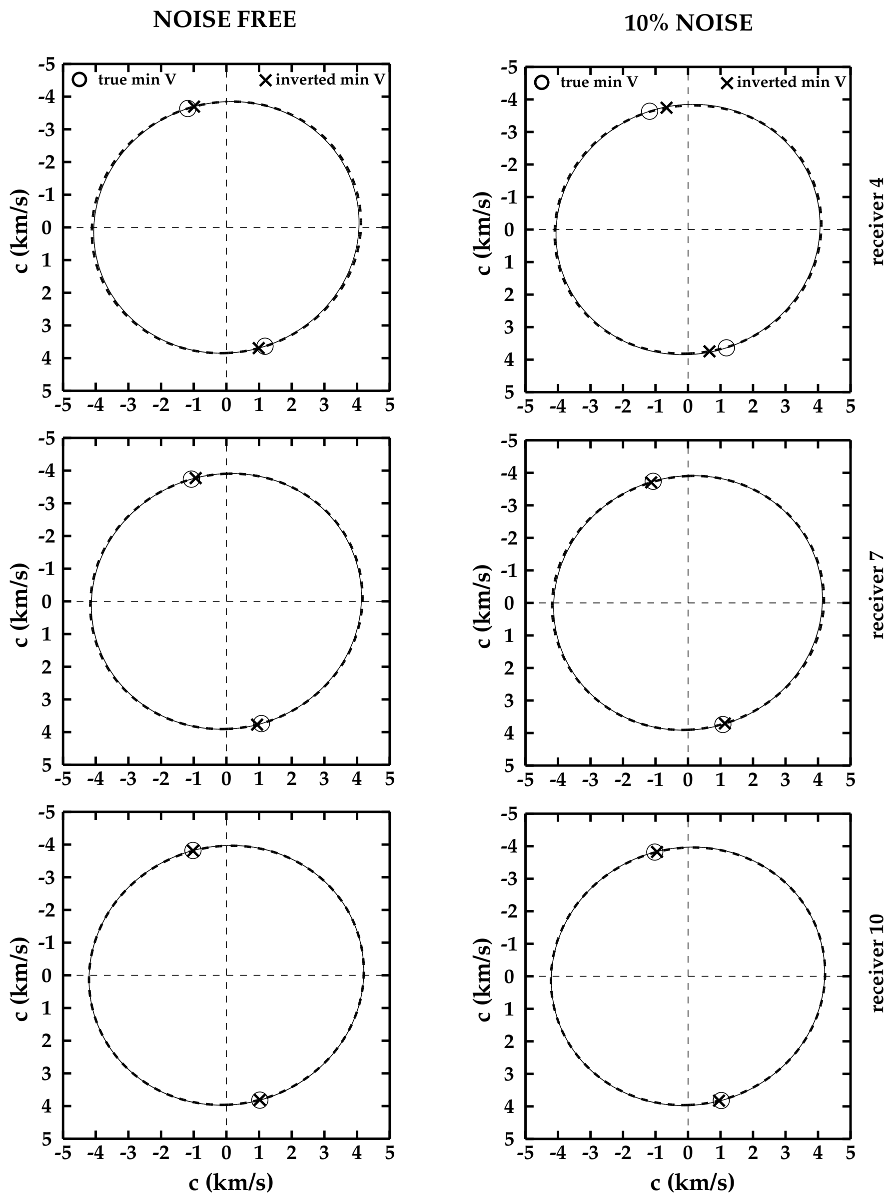

Figure 5

MODEL TI-16

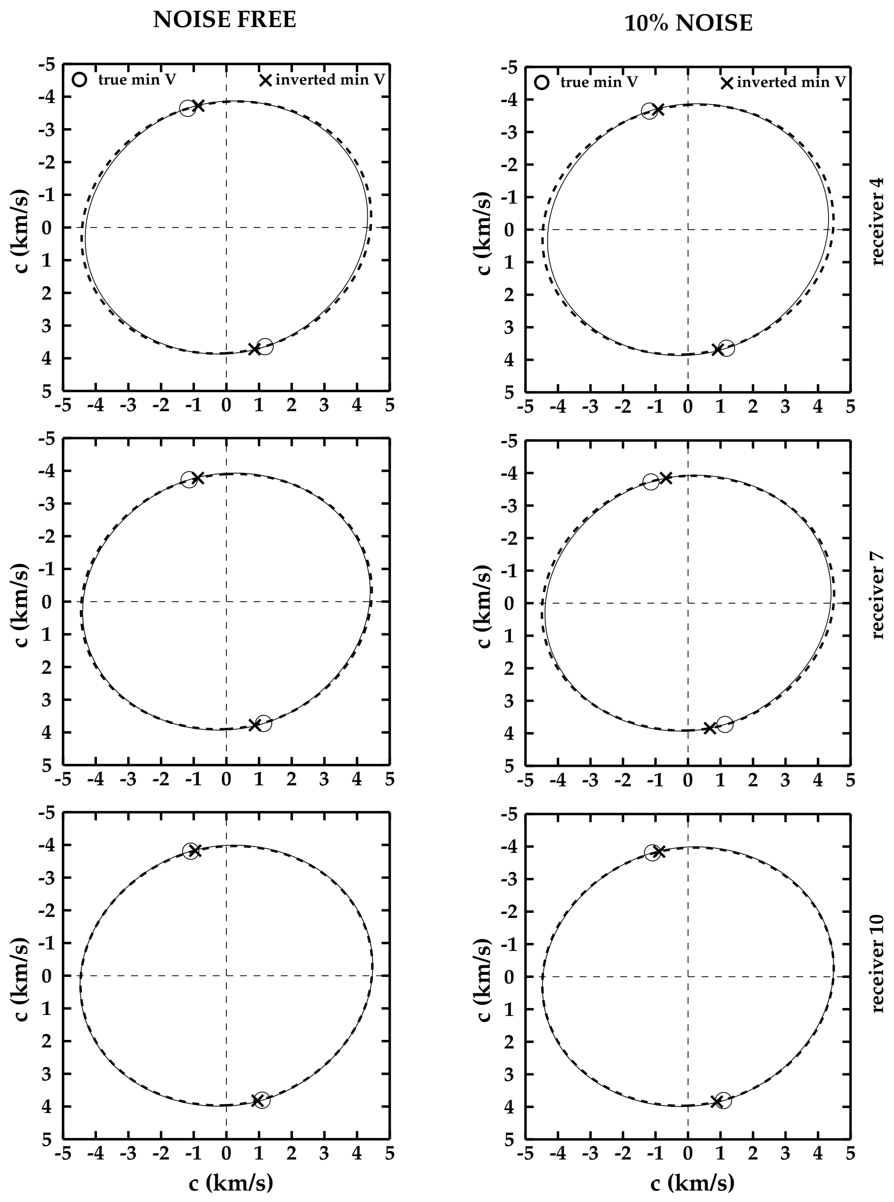

Figure 6

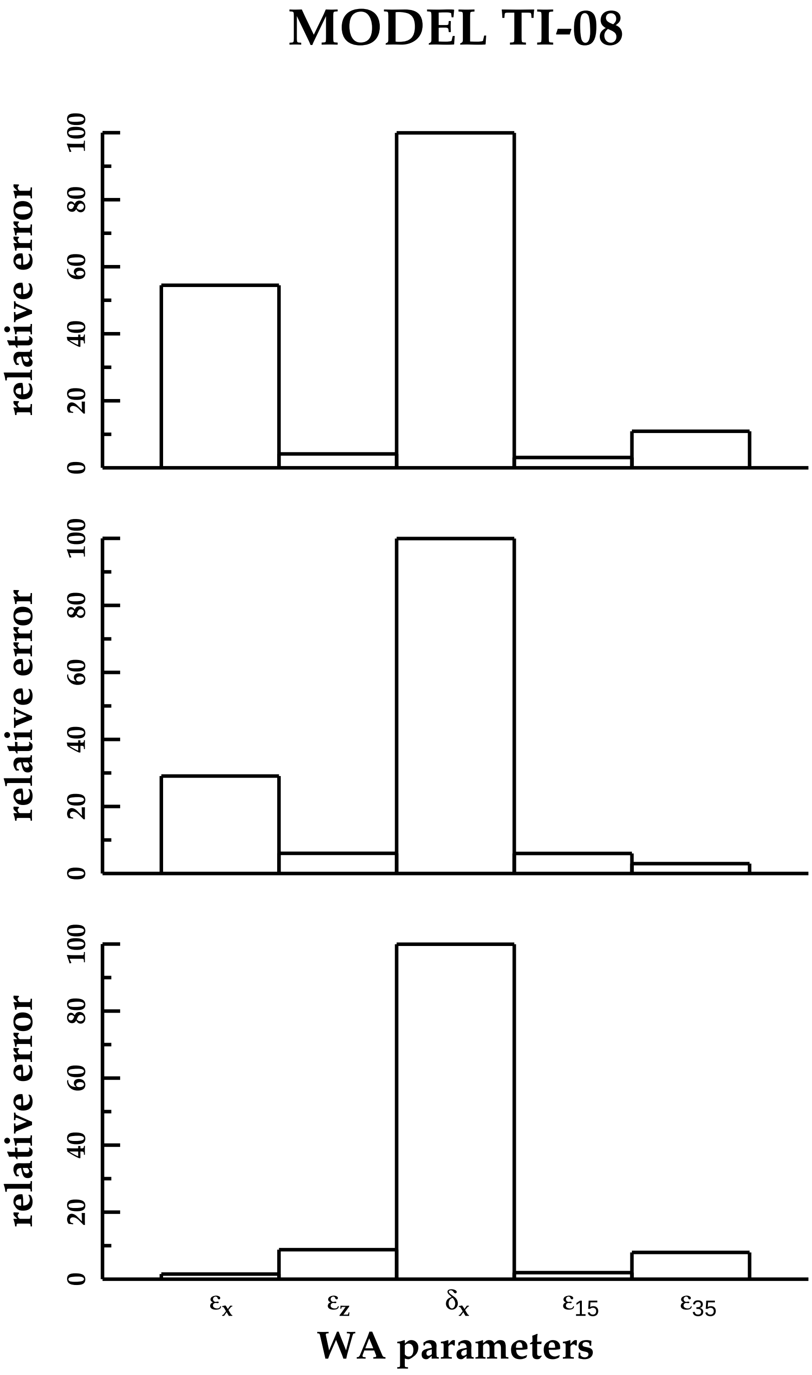
MODEL TI-08
relative error
0
20
40
60
80
100
relative error
0
20
40
60
80
100
relative error
0
20
40
60
80
100
εx
εz
δx
ε15
ε35
WA parameters

Figure 7

MODEL TI-08

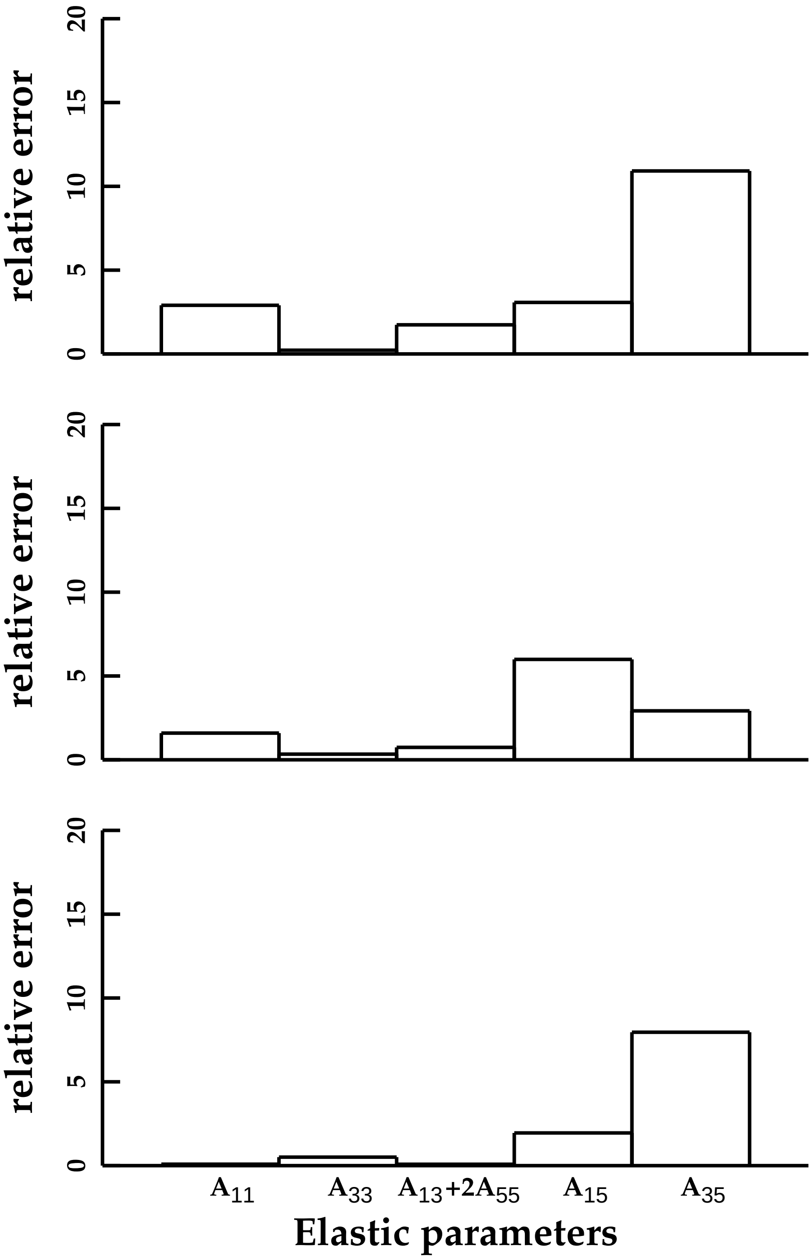

Figure 8

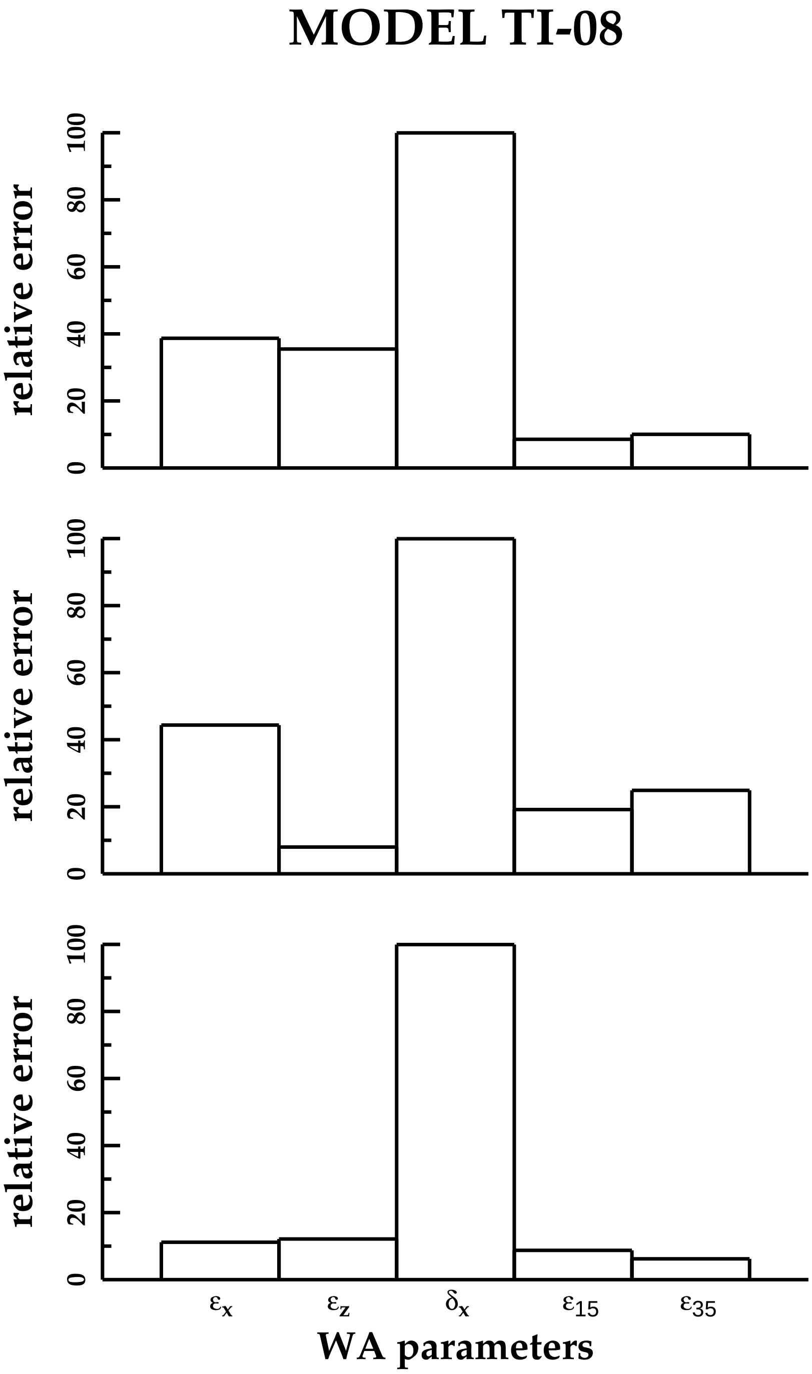
MODEL TI-08
relative error
0
20
40
60
80
100
relative error
0
20
40
60
80
100
relative error
0
20
40
60
80
100
εx
εz
δx
ε15
ε35
WA parameters

Figure 9

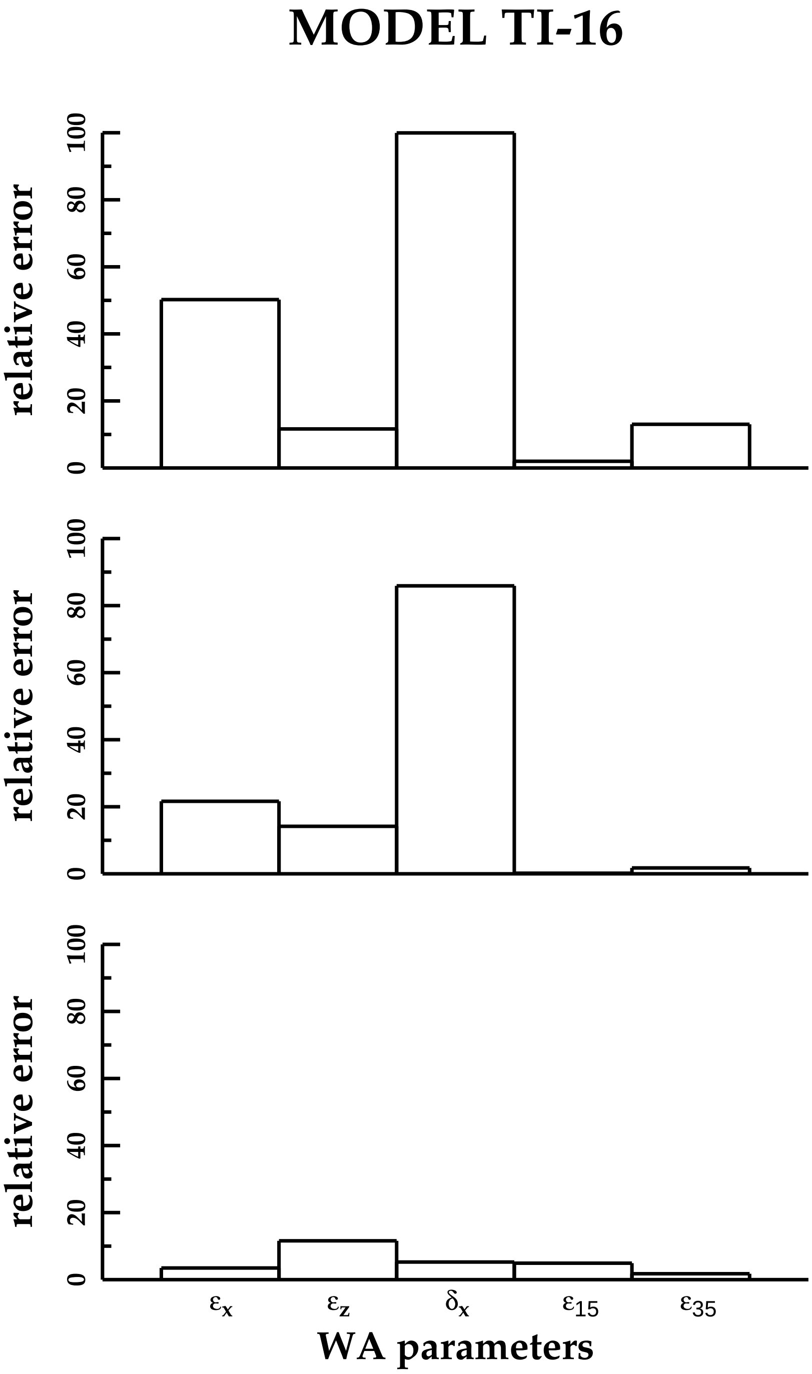
MODEL TI-16
relative error
0
20
40
60
80
100
relative error
0
20
40
60
80
100
relative error
0
20
40
60
80
100
ε_x
ε_z
δ_x
ε_{15}
ε_{35}
WA parameters

Figure 10

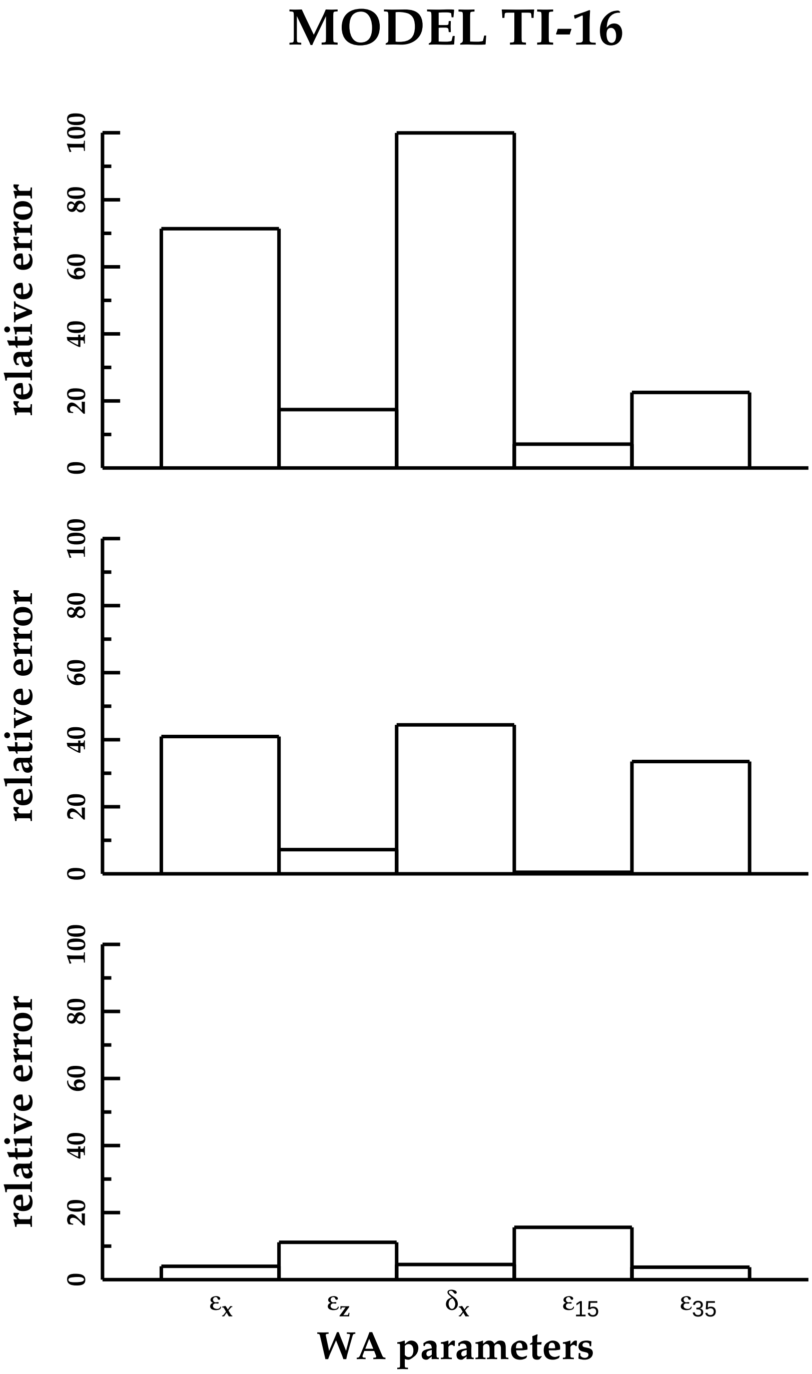

MODEL TI-16
relative error
0
20
40
60
80
100
εx
εz
δx
ε15
ε35
WA parameters

Figure 11

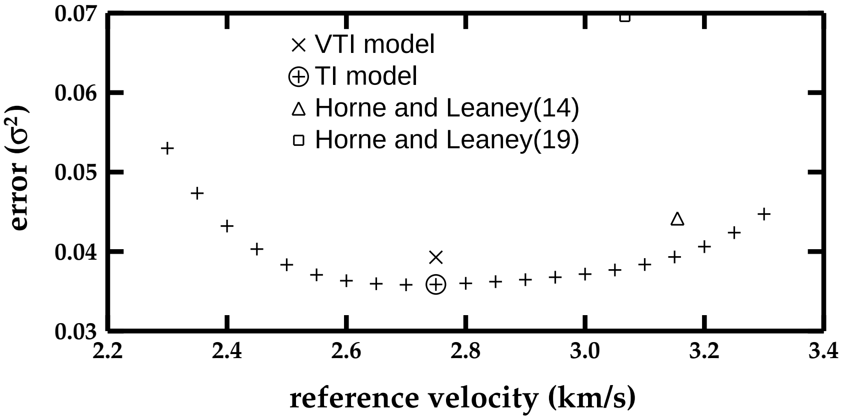
0.07
0.06
0.05
0.04
0.03
error (σ^2)
2.2
2.4
2.6
2.8
3.0
3.2
3.4
reference velocity (km/s)
VTI model
TI model
Horne and Leaney(14)
Horne and Leaney(19)

Figure 12

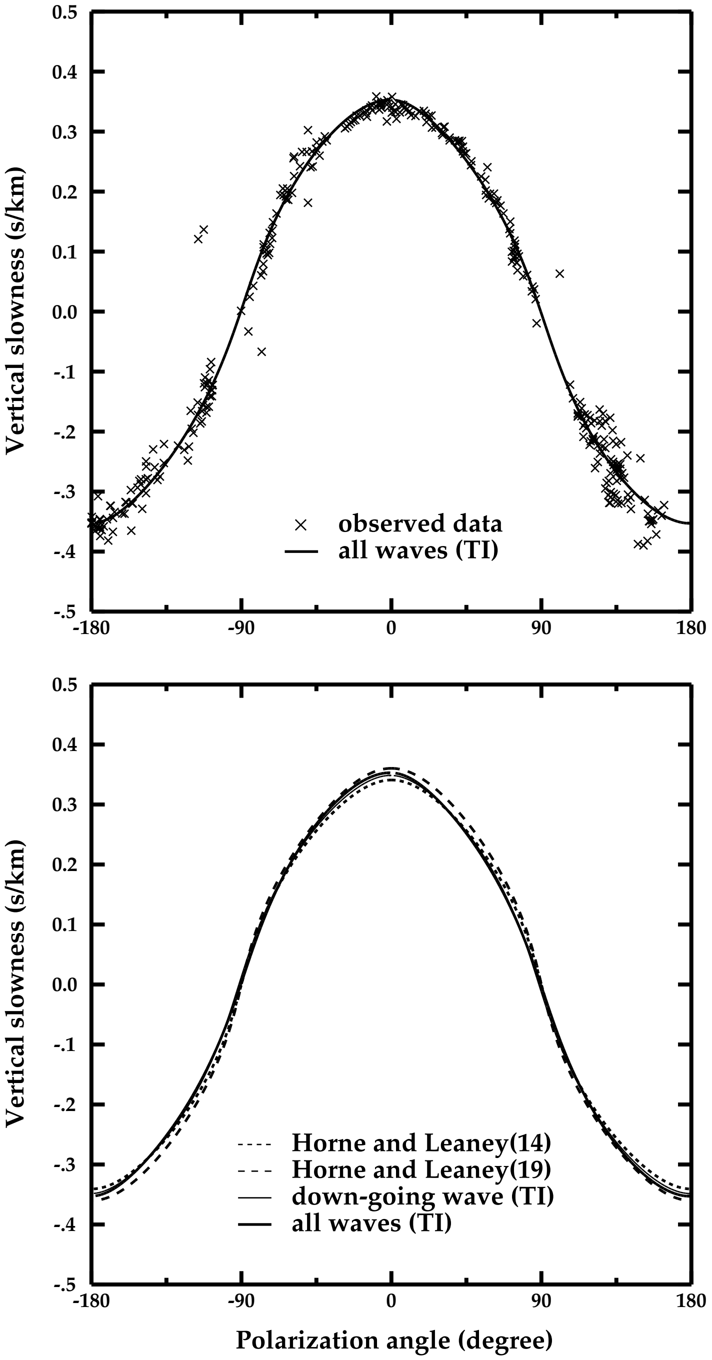
Vertical slowness (s/km)
observed data
all waves (TI)
Horne and Leaney(14)
Horne and Leaney(19)
down-going wave (TI)
all waves (TI)
Polarization angle (degree)

Figure 13

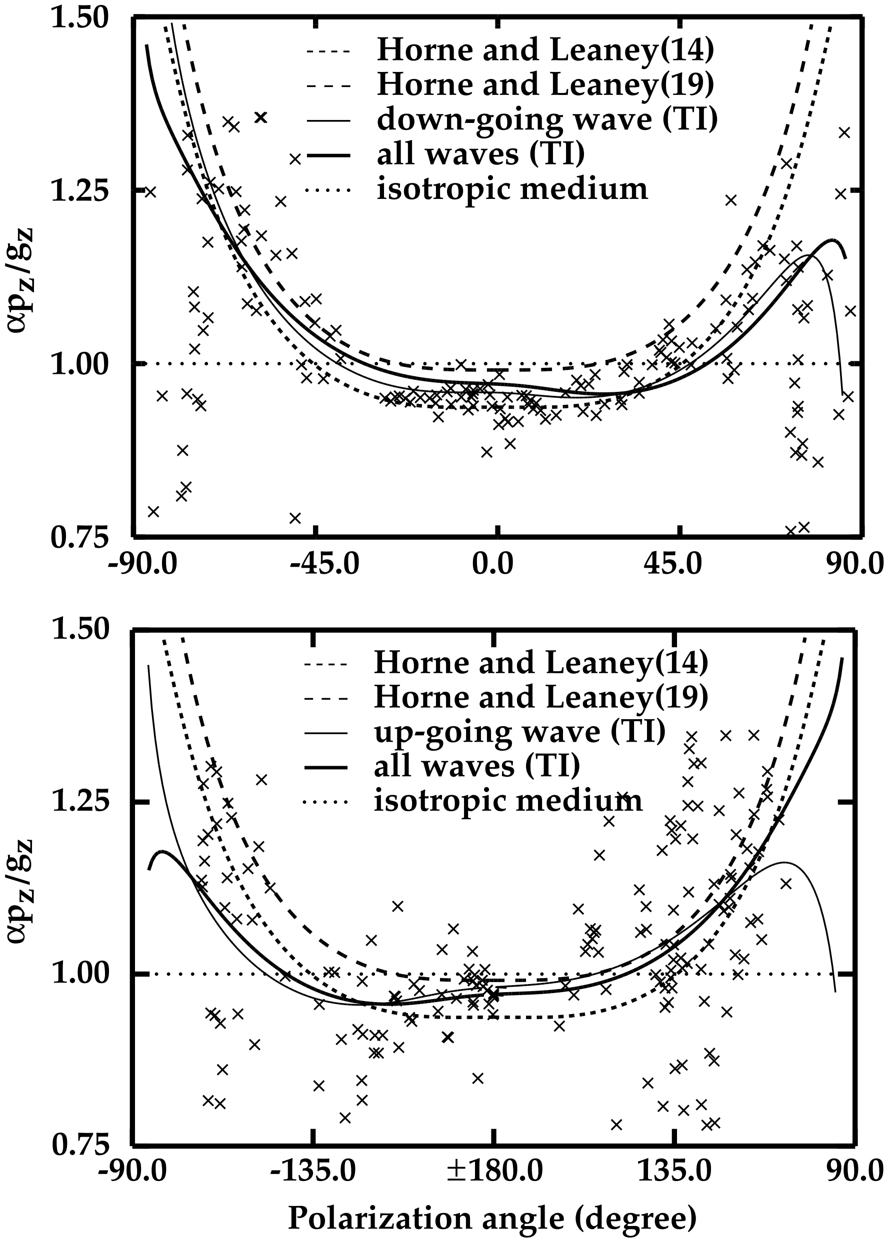

Horne and Leaney(14)
Horne and Leaney(19)
down-going wave (TI)
all waves (TI)
isotropic medium
$\alpha p_z/g_z$
1.50
1.25
1.00
0.75
-90.0
-45.0
0.0
45.0
90.0
Horne and Leaney(14)
Horne and Leaney(19)
up-going wave (TI)
all waves (TI)
isotropic medium
$\alpha p_z/g_z$
1.50
1.25
1.00
0.75
-90.0
-135.0
±180.0
135.0
90.0
Polarization angle (degree)

Figure 14

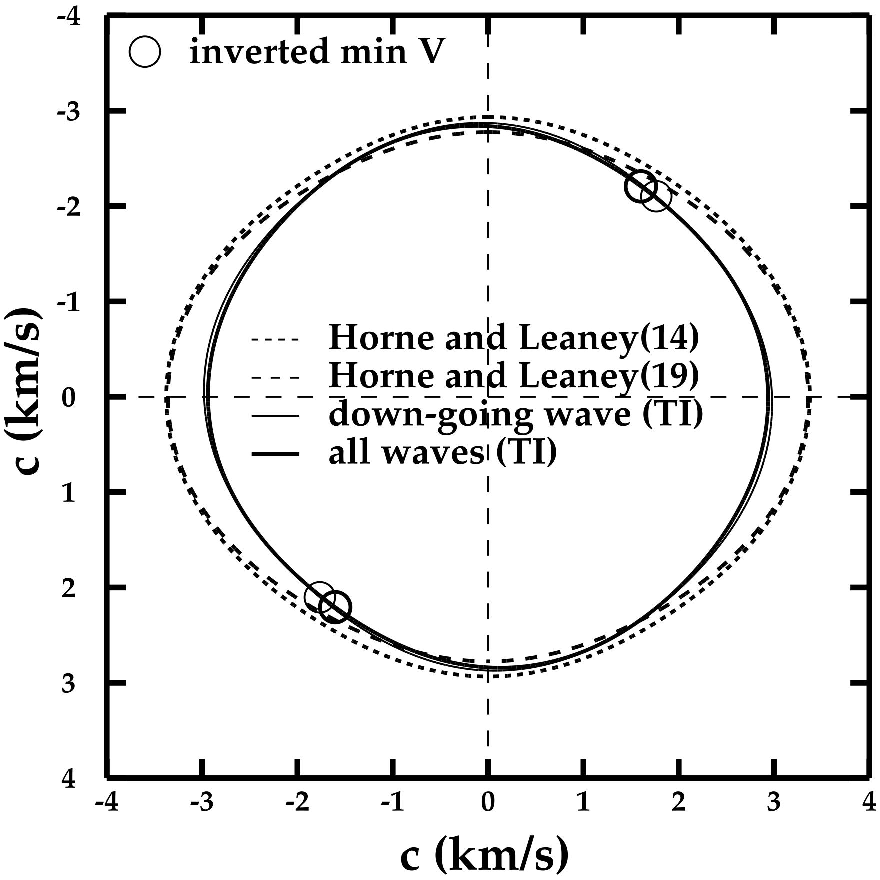
inverted min V
Horne and Leaney(14)
Horne and Leaney(19)
down-going wave (TI)
all waves (TI)
c (km/s)
c (km/s)
-4
-3
-2
-1
0
1
2
3
4
-4
-3
-2
-1
0
1
2
3
4

Figure 15

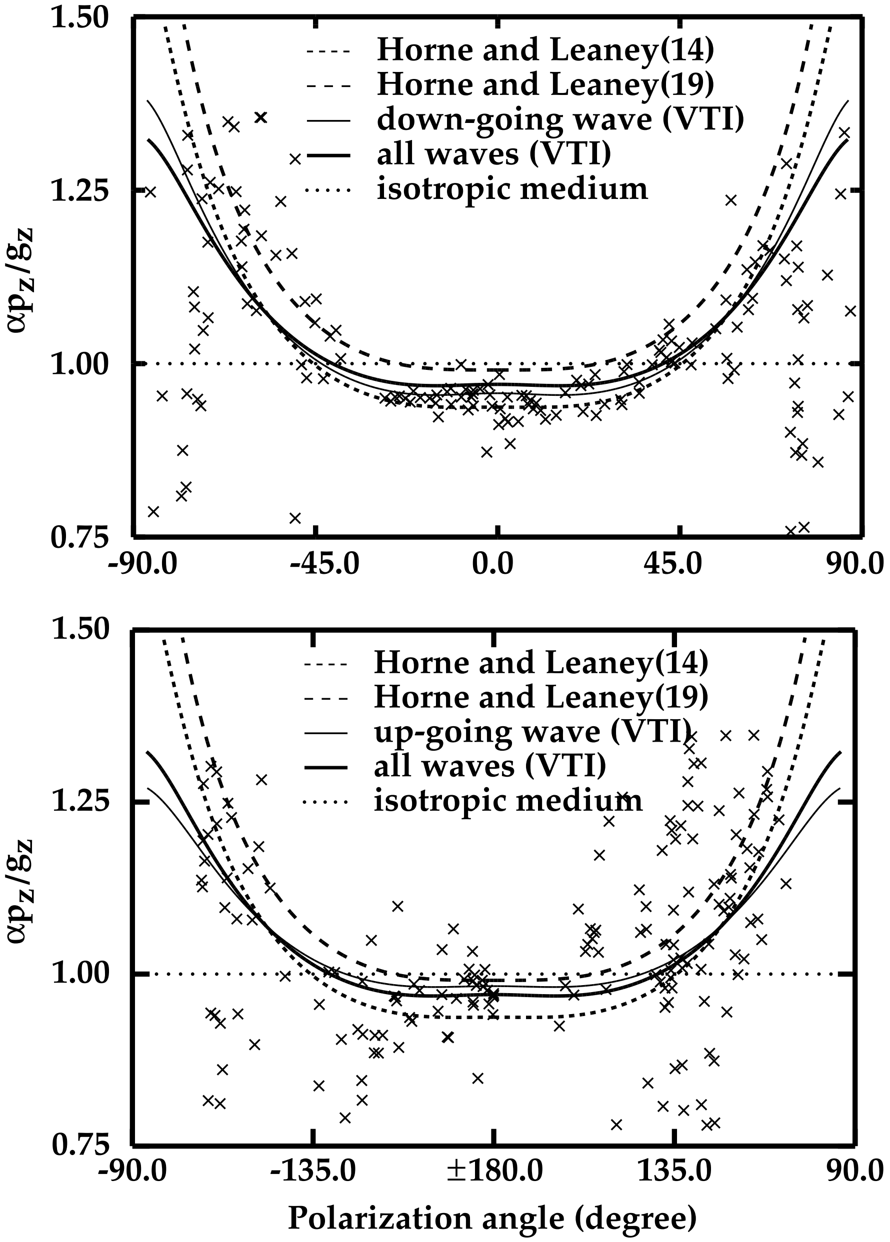

1.50
1.25
1.00
0.75
$\alpha p_z/g_z$
Horne and Leaney(14)
Horne and Leaney(19)
down-going wave (VTI)
all waves (VTI)
isotropic medium
-90.0
-45.0
0.0
45.0
90.0
1.50
1.25
1.00
0.75
$\alpha p_z/g_z$
Horne and Leaney(14)
Horne and Leaney(19)
up-going wave (VTI)
all waves (VTI)
isotropic medium
-90.0
-135.0
±180.0
135.0
90.0
Polarization angle (degree)

Figure 16

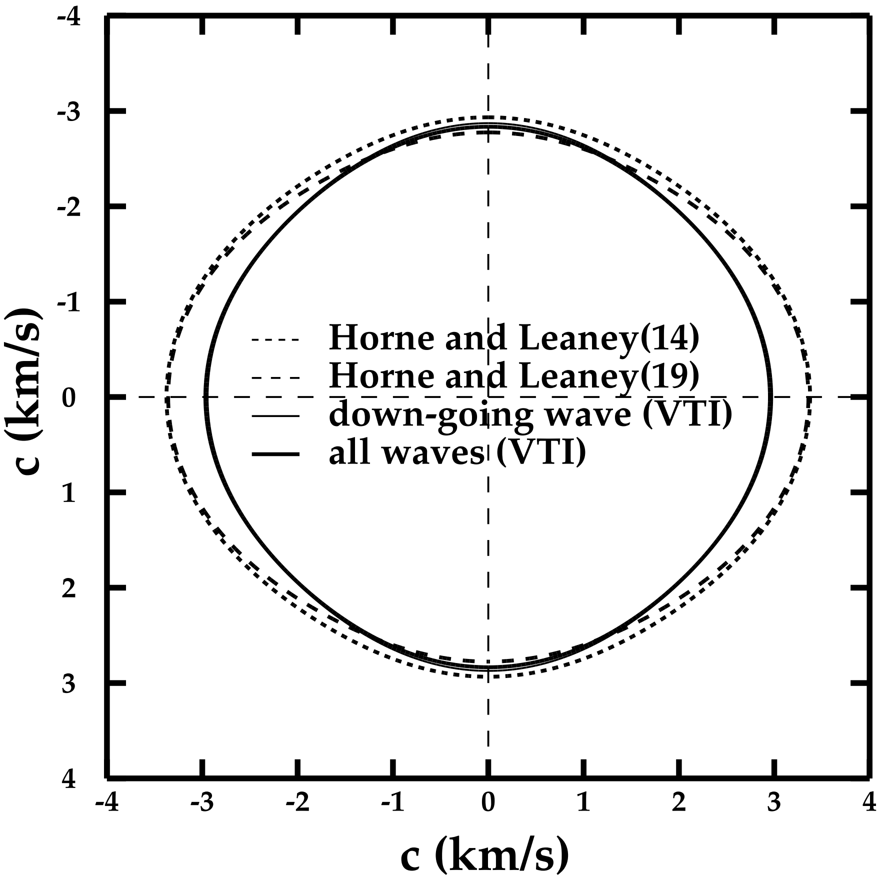
-4
-3
-2
-1
0
1
2
3
4
c (km/s)
Horne and Leaney(14)
Horne and Leaney(19)
down-going wave (VTI)
all waves (VTI)
-4
-3
-2
-1
0
1
2
3
4
c (km/s)

Figure 17